Supporting Information

Self-Evolutionary Recycling of Flame-retardant Polyurethane Foam Enabled by Controllable Catalytic Cleavage

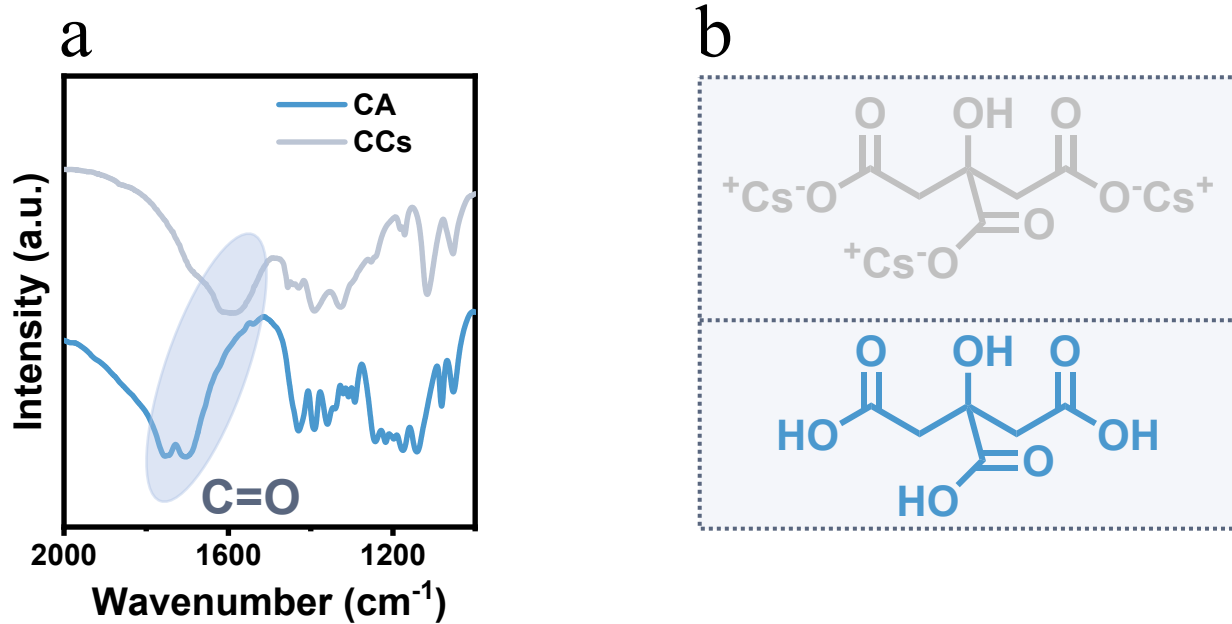Dan-Xuan Fang[1], Ming-Jun Chen[2], Fu-Rong Zeng[1], Shuai-Qi Guo[1], Lei He[1], Bo-Wen Liu[1], Sheng-Chao Huang[3], Hai-Bo Zhao[1]*, Yu-Zhong Wang[1]*

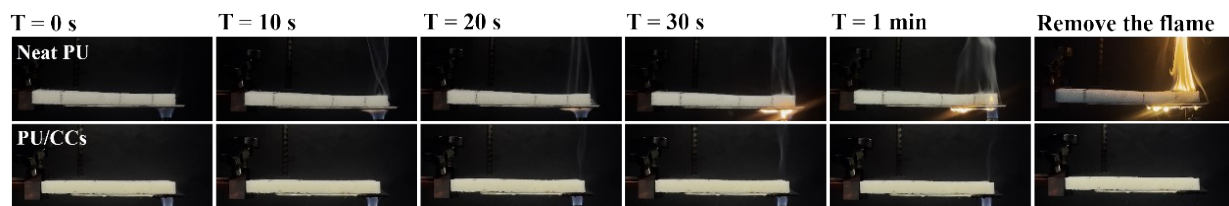**This PDF file includes:**

Supplementary Text
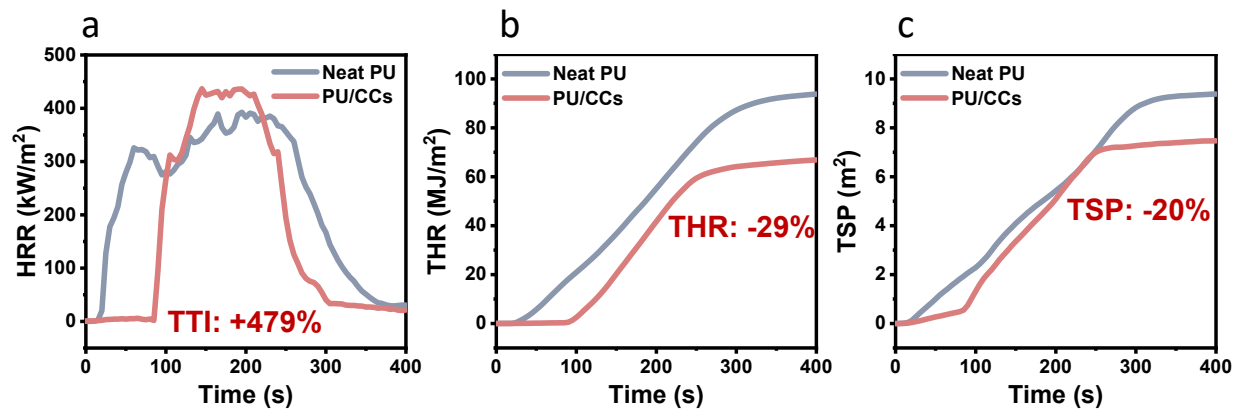
Figs. S1 to S18

Tables S1 to S9

Fig. S1. FTIR characterization. FTIR (a) and (b) structure of CA and CCs.

The carbonyl group of carboxylic acid in citric acid has a strong absorption peak at 1742 cm^{-1}, while the carbonyl absorption peak of cesium citrate appears at 1588 cm^{-1}.

T = 0 s	T = 10 s	T = 20 s	T = 30 s	T = 1 min	Remove the flame

Neat PU

PU/CCs

Fig. S2. ASTM-D4986 tests of neat PU and PU/CCs.

Fig. S3. The results of the cone calorimetry tests. (a)Heat release rates (HRR), (b) total heat release (THR) and (c) total smoke production (TSP) curves obtained from cone calorimetry at the heat flux of 35 kW/m^2.
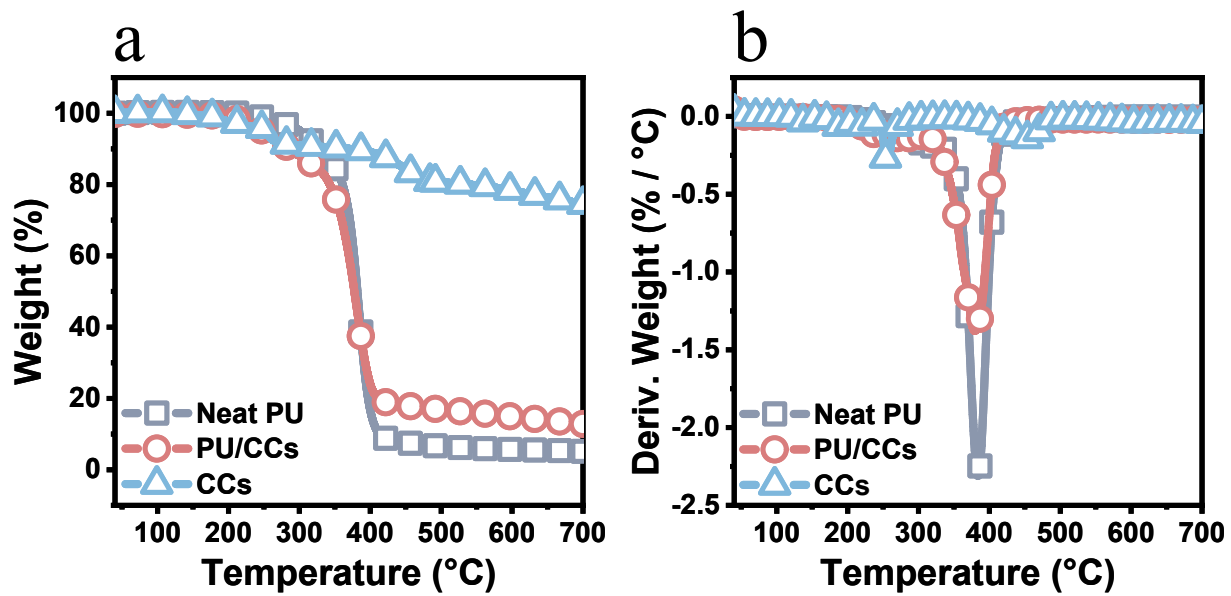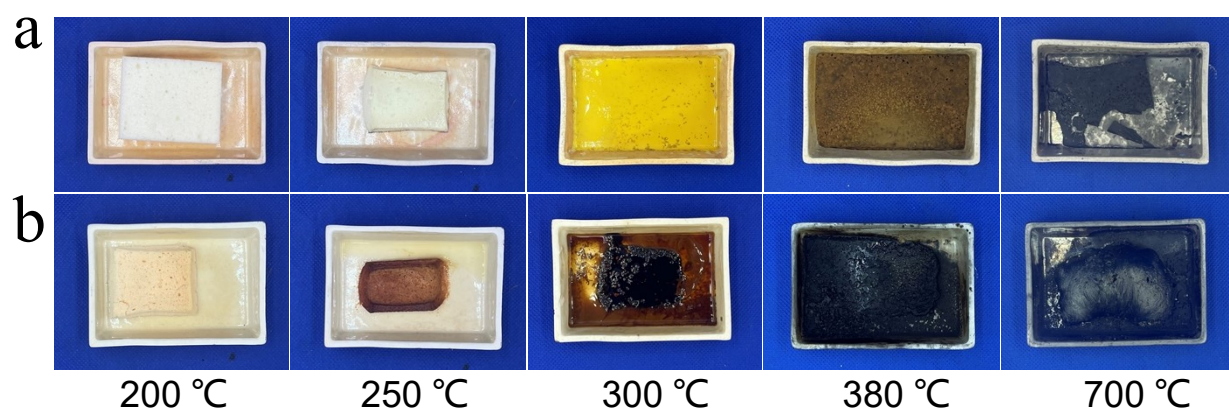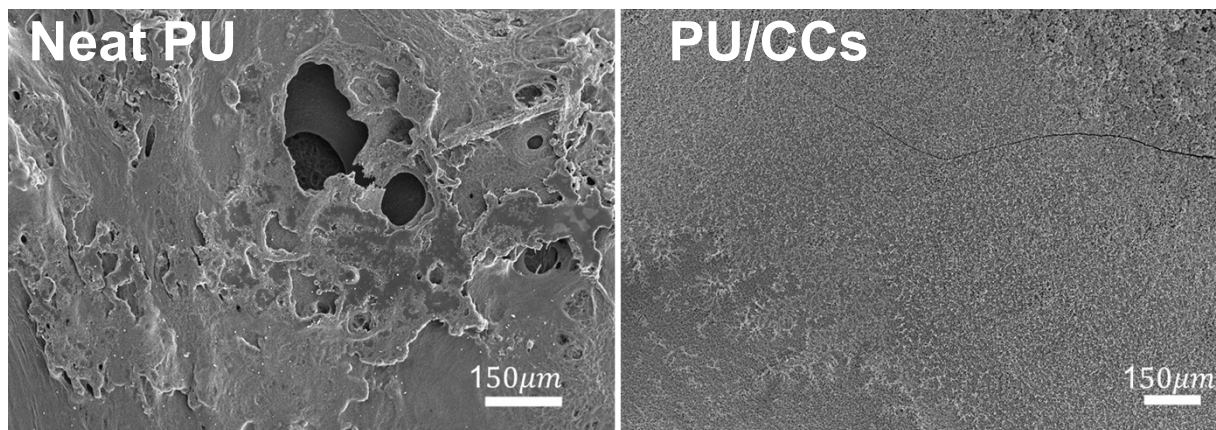
Fig. S4. TG characterization of CCs, neat PU and PU/CCs. (a) TG and (b) DTG.

Fig. S5. Macro-images of carbon residue in a tube furnace of PU at different temperatures under a nitrogen atmosphere. Neat PU (a) and PU/CCs (b).

Fig. S6. Microstructure of residue char. SEM images of residue char of neat PU and PU/CCs at 700 °C under a nitrogen atmosphere in a tube furnace.

The residual char in a tube furnace of PU at different temperatures under a nitrogen atmosphere was collected to understand the condensed flame-retardant mechanism by SEM (**Fig. S6**). The residue char of PU/CCs, compared with neat PU, was capable of earlier pyrolysis and finally caused a smooth and compacted surface, which was expected to inhibit mass and heat transfer during the burning stage.
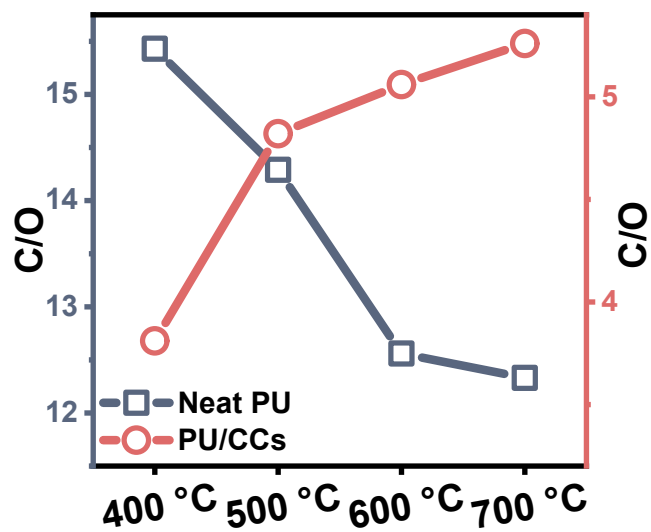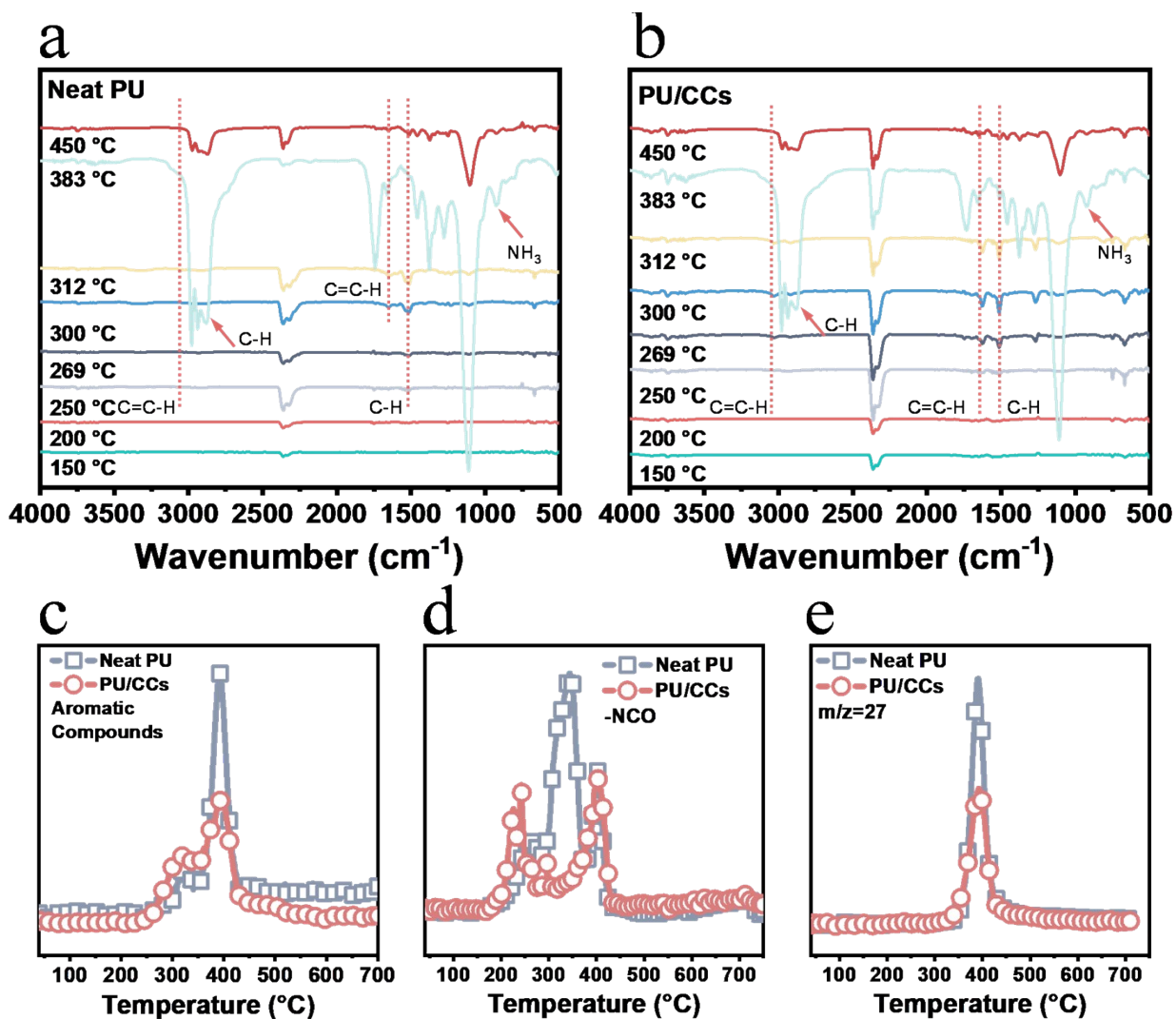
Fig. S7. XPS data of the ratio of carbon to oxygen of neat PU and PU/CCs at different temperatures under a nitrogen atmosphere in a tube furnace.

Fig. S8. Gas flame-retardant mechanism. TG-IR spectra of gaseous pyrolysis products of neat PU (a) and PU/CCs (b) at different temperatures. Intensity of selected peaks: Aromatic compounds (c), -NCO (d) and HCN from TG-MS (e) for thermal degradation products of neat PU and PU/CCs.

To further investigate the flame-retardant mechanism gas phase, TG-IR and TG-MS characterization was conducted to analyse the evolved gas products of neat PU and PU/CCs during the whole thermal degradation process. **Fig. S8** presents the TG-IR and TG-MS spectra of the released volatiles at selected temperatures. The neat PU and PU/CCs presented the similar characteristic signals. However, compared with the neat PU, the PU/CCs showed a lower characteristic absorption intensity of flammable volatile products, such as aromatic compounds. The adding of CCs, on the other hand, facilitated the breakage of carbamate bonds, and the generation temperature of both HCN and -NCO was significantly reduced. Therefore, the CCs can decrease the release of toxic gas and flammable volatiles, exhibiting efficient gas-phase flame retardancy.
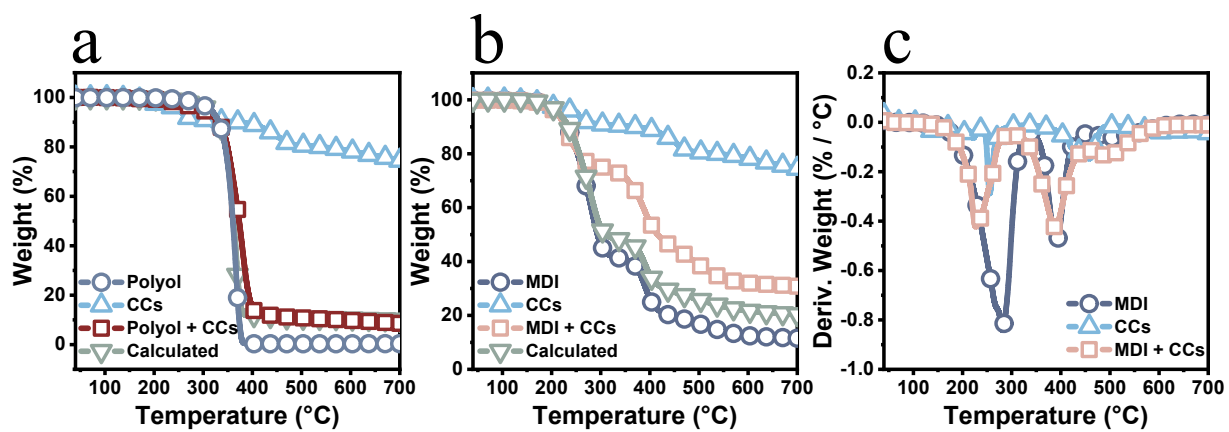
Fig. S9. TG characterization of CCs, CCs with polyols and CCs with MDI. TG curves for the calculated and actual values of polyol (a) or MDI (b) with CCs. and (c) DTG under a nitrogen atmosphere.
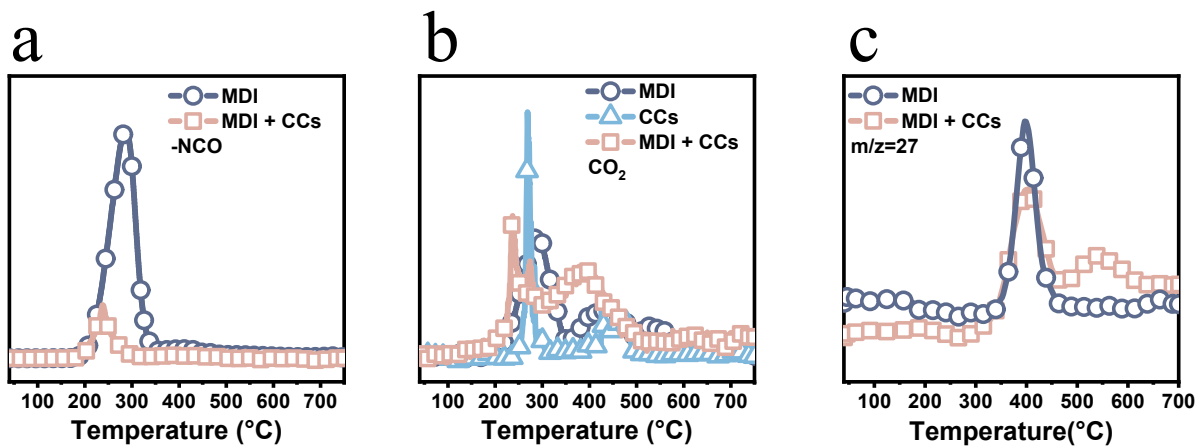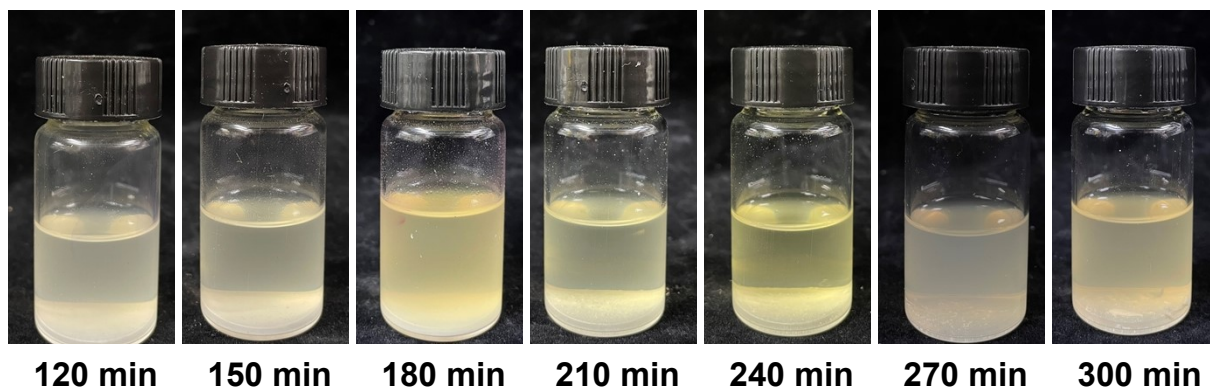
Fig. S10. Gas phase characterization of MDI and MDI with CCs. TG-IR intensity of selected peaks: NCO (a) and CO_2 (b). Decomposition product, HCN (c), tracked by TG-MS for MDI and MDI with CCs.
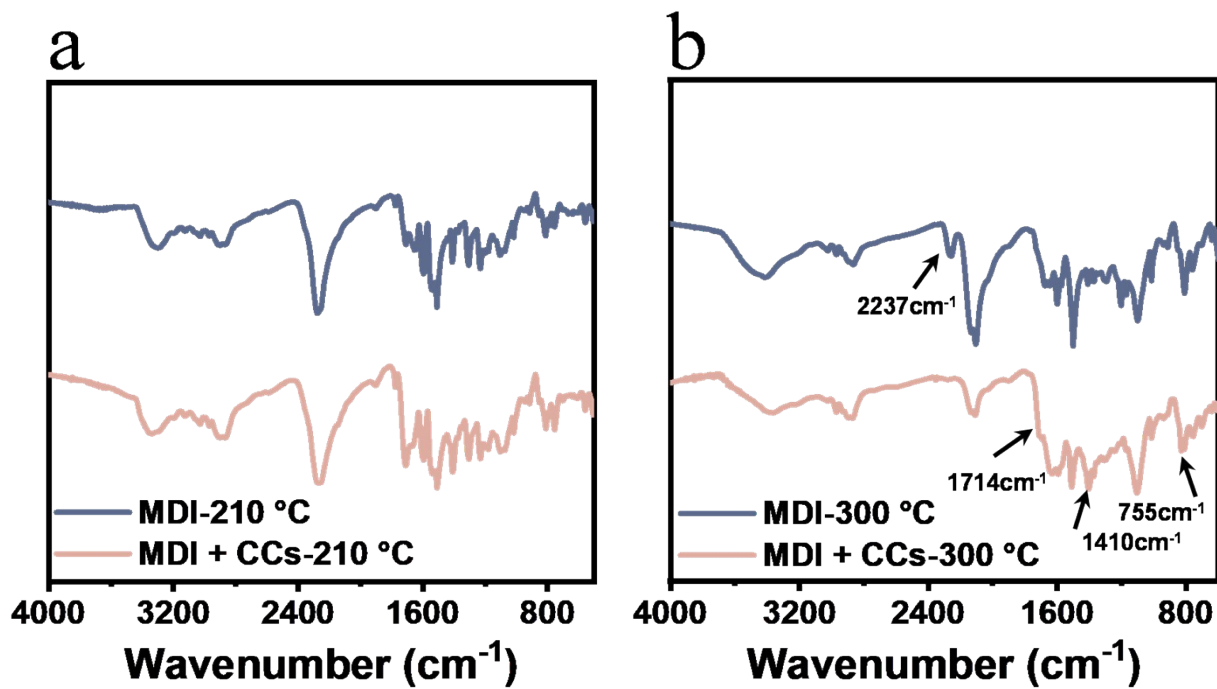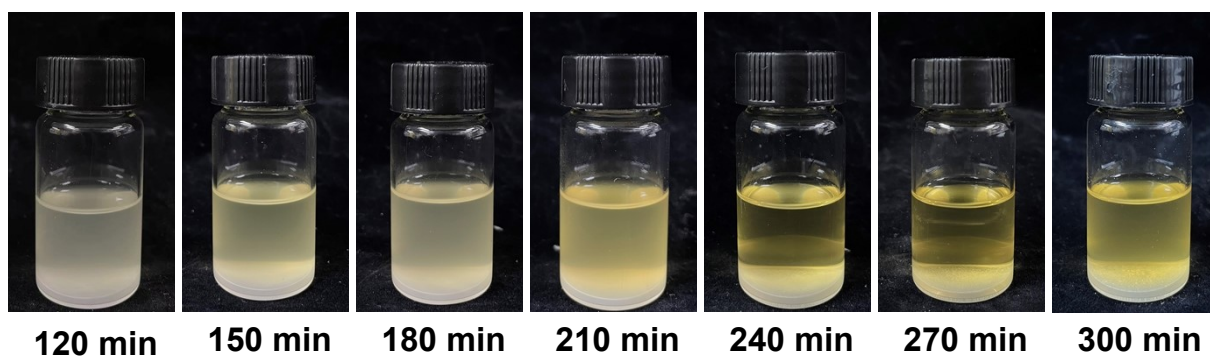
Fig. S11. FTIR characterization. FTIR spectra of the decomposition products of MDI (a) and MDI with CCs (b) at 210 °C and 300 °C under a nitrogen atmosphere in a tube furnace.

Neat PU

| 120 min | 150 min | 180 min | 210 min | 240 min | 270 min | 300 min |

PU/CCs

| 120 min | 150 min | 180 min | 210 min | 240 min | 270 min | 300 min |

Fig. S12. Screening for optimal degradation time. Digital photograph of the dissolution of degradation products in methanol to screen for optimal degradation time (neat PU: 240 minutes, PU/CCs: 270 minutes).

The products of alcoholysis at different degradation time were dissolved in organic solvents, and the reaction endpoints were judged according to their degree of dissolution. Here the optimal degradation condition for neat PU was determined to be a 240-minute reaction at 220 °C. And for PU/CCs was determined to be a 270-minute reaction at 180 °C.
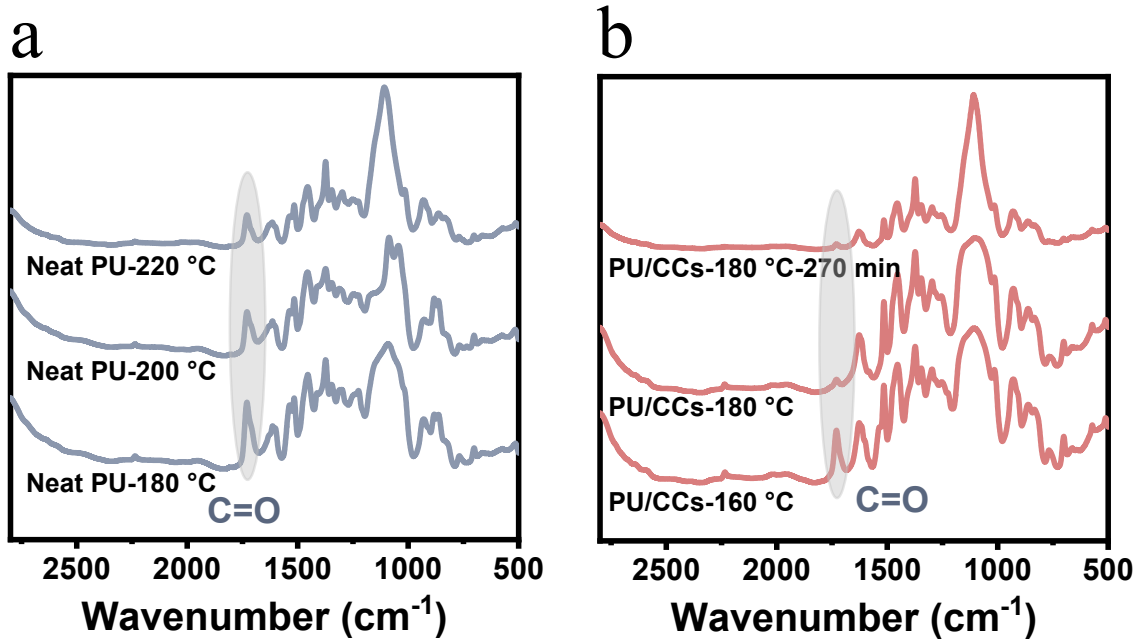
Fig. S13. FTIR characterization. FTIR spectra of the upper phase from split-phase alcoholysis of neat PU (a) and PU/CCs (b) under different degradation conditions.
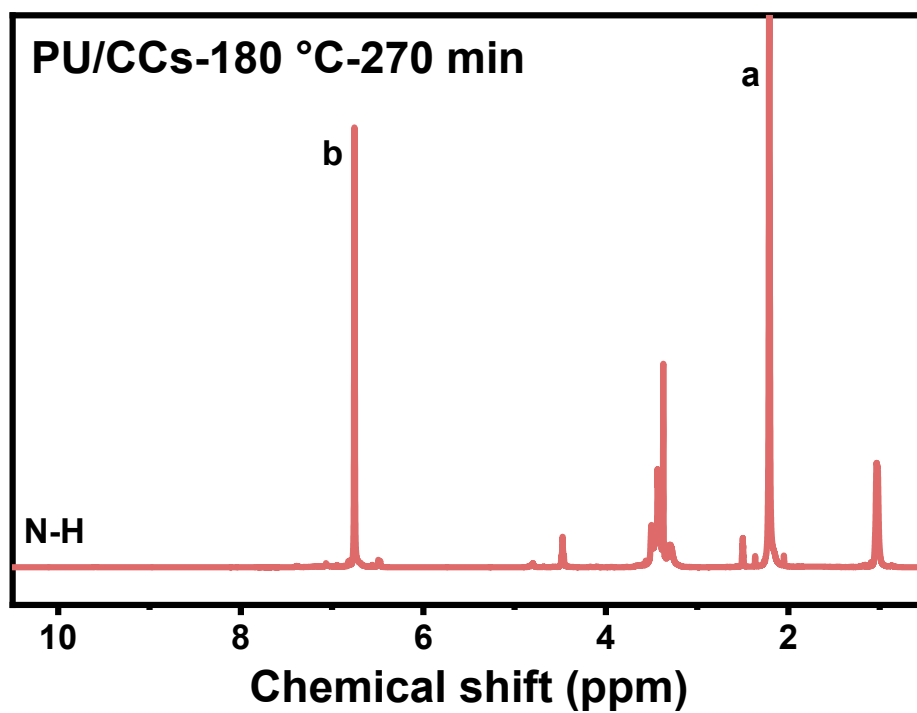
Fig. S14. NMR characterization. ^{1}H NMR spectra of the upper phase from split-phase alcoholysis of PU/CCs under the best degradation conditions.
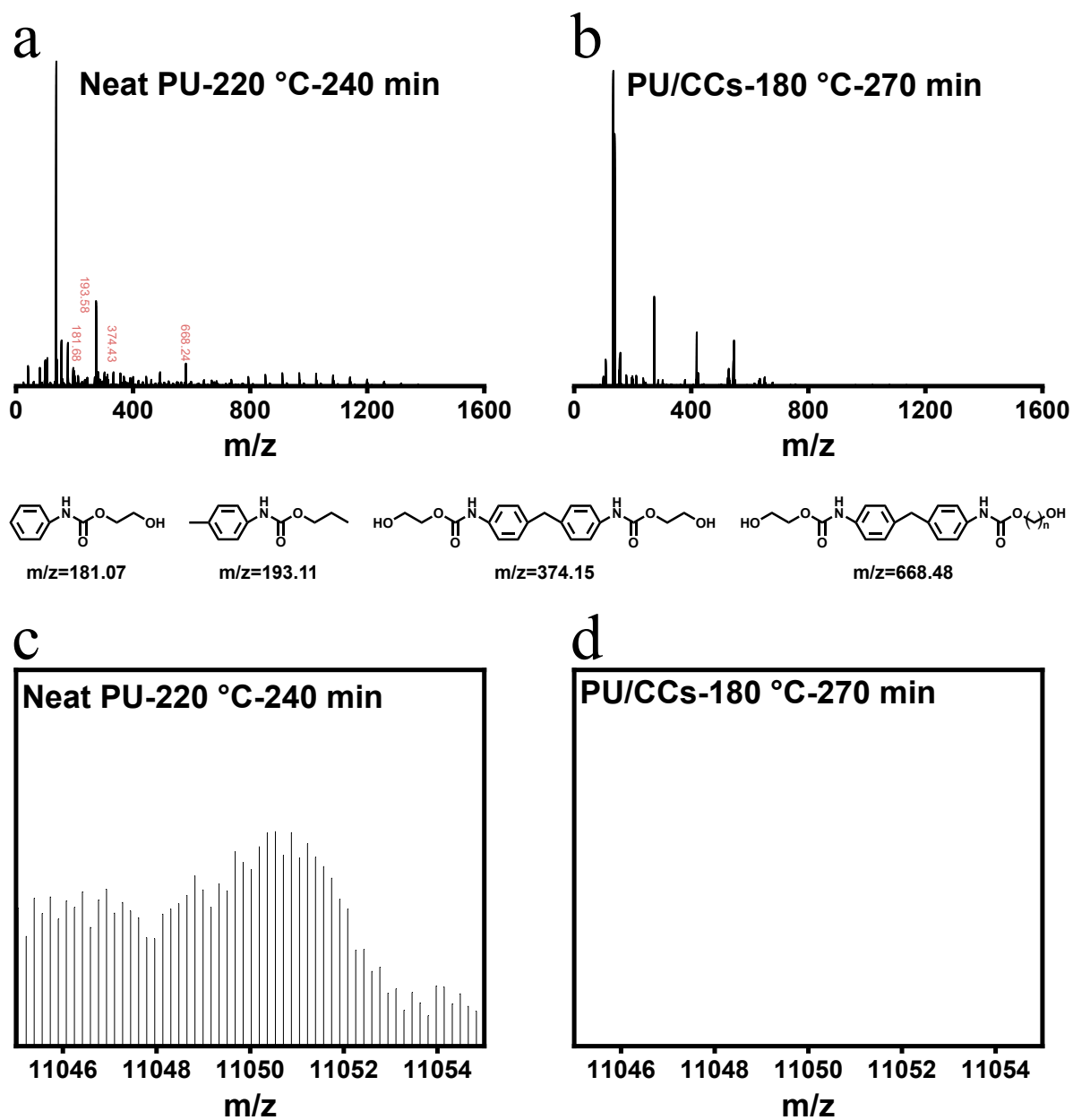
Fig. S15. Characterization of the purity of degradation products. MALDI-TOF mass spectra of neat PU and PU/CCs under optimal degradation conditions in the low mass region (a-b) and high mass region (c-d).
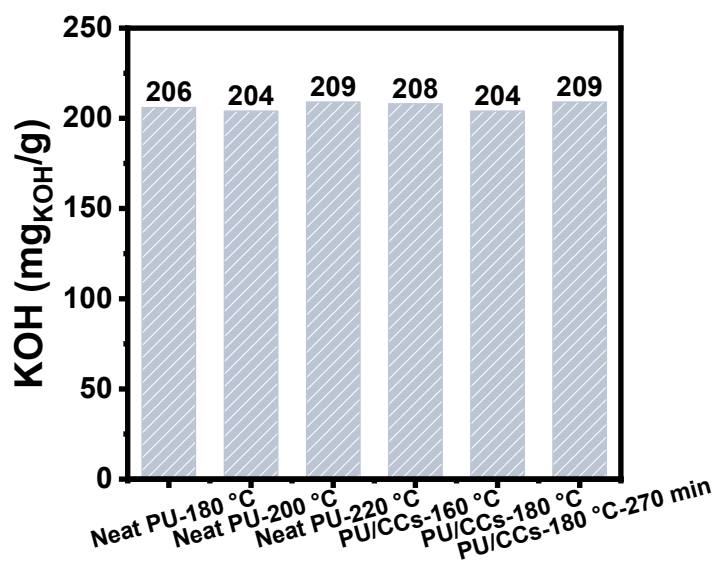
Fig. S16. Hydroxyl values test. Hydroxyl values of recycled polyols from different degradation conditions.
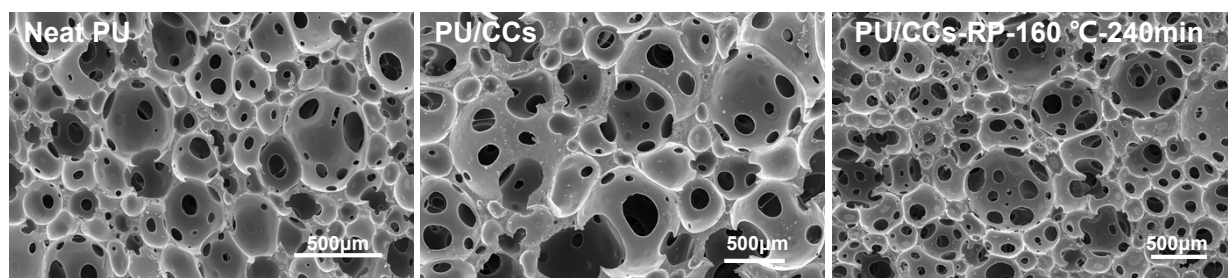
Fig. S17. Surface microstructure of neat PU and coated PU/CCs. Scanning electron microscope images of neat PU and PU/CCs and PU/CCs-RP at 160 °C for 240 minutes.
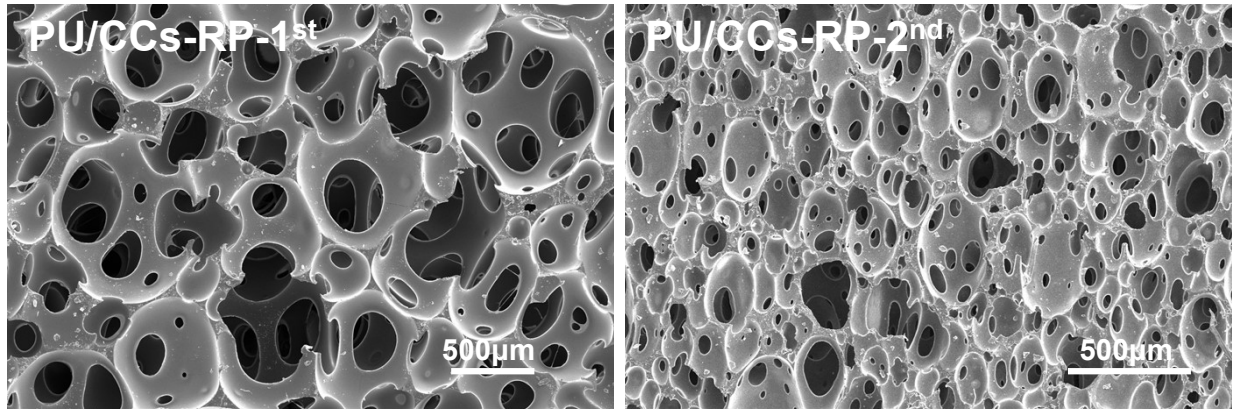
Fig. S18. Surface microstructure of Newly prepared PU. Newly prepared polyurethane foams with multiple recycled polyols.

Table S1. Detailed AAS data of Cs.

AAS	Test value (%)	Theoretical value (%)
Cs	63.5	67.8

Table S2. Test results of horizontal burning test.

Criteria Conditions	Neat PU	PU/CCs
Afterflame time	96 s	0 s
Afterglow time for each individual specimen	96 s	0 s
Cotton indicator ignited by flaming particles or drops	Yes	None
Damaged length for each individual specimen	150 mm	1mm

Table S3. Detailed combustion data from cone calorimetry at the heat flux of 25 kW/m² of neat PU and PU/CCs.

Sample	TTI (s)	tP (s)	PHRR$_{max}$ (kW/m²)	PHRR$_1$ (kW/m²)	PHRR$_2$ (kW/m²)	THR[a] (MJ/m²)	FIGRA[b]	TSP[c] (m²)	char yield (%）
Neat PU	17	245	325	243	325	87	4.18	44	6
PU/CCs	61	440	409	90	409	74	1.22	9	13

[a] Total heat release.

[b] Fire Growth Rate Index：Maximum value of the ratio of the heat release rate to its corresponding time.

[c] Total smoke production.

Table S4. Detailed combustion data from cone calorimetry at the heat flux of 35 kW/m² of neat PU and PU/CCs.

Sample	TTI (s)	tP (s)	PHRR$_{max}$ (kW/m²)	THR (MJ/m²)	FIGRA	TSP (m²)	char yield (%)
Neat PU	14	195	392	95	5.92	9.47	4
PU/CCs	81	145	436	66	2.15	6.98	9

Table S5. Detailed TG data of CCs, neat PU and PU/CCs in a nitrogen atmosphere at a heating rate of 10 °C/min.

Sample/N$_2$	T$_{5\%}$ (°C)	T$_{max}$ (°C)	CY (288 °C/%)	CY (436 °C/%)	CY (700 °C/%)
CCs	253	257/460	91	89	74
Neat PU	301	385	96	8	5
PU/CCs	248	380	90	18	13

Table S6. Detailed TG data of MDI, CCs, MDI with CCs and calculated values in a nitrogen atmosphere at a heating rate of 10 °C/min.

Sample	$T_{5\%}$ (°C)	T_{max1} (°C) /R_{max1} (%/°C)	T_{max2} (°C) /R_{max2} (%/°C)	CY (300 °C/%)	CY (400 °C/%)	CY (600 °C/%)	CY (700 °C/%)
MDI	214	281/0.84	390/0.49	46	26	12	12
CCs	253	255/0.29	455/0.14	91	89	78	74
MDI+CCs	211	226/0.42	389/0.42	75	55	32	31
Calculated	215			53	35	22	20

Table S7. Detailed AAS data of Cs before and after dry and wet aging tests.

AAS	Before aged (%)	After dry aged[a] (%)	After humid aged (%)
Cs	5.37	6.32	4.92

[a] During the dry heat aging process, the mass loss was 10.7%, which coincided with the trend of cesium content.

Table S8. GPC analysis results.

Sample	Mn/g.mol^{-1}	Mw/g.mol^{-1}	Polydispersity Index
330N+POP-1	49588	79253	1.60
330N+POP-2	5215	7874	1.51
Neat PU-220 °C -240 min	6205	8697	1.40
PU/CCs-160 °C -240 min	4938	7735	1.57
PU/CCs-180 °C -270 min	6109	8127	1.33

Table S9. ^{1}H NMR integration results.

Sample	Mesitylene-CH$_3$	N-H bond
Neat PU-220 °C-240 min	1	0.0042
PU/CCs-160 °C-240 min	1	0.0038
PU/CCs-180 °C-270 min	1	0.0014